Fabrication, investigation and modification of magnetic states in nano-scale patterned cobalt films by using scanning ion microscopy with polarization analysis (SIMPA)

Jian Li, Carl Rau *

Department of Physics and Astronomy, Rice Quantum Institute and Smalley Institute for Nanoscience and Technology, Rice University, Houston, TX 77251, USA

Available online 20 February 2007

Abstract

Focused ion beam (FIB) lithography is used to fabricate patterned Co nano-elements from ultra-thin (30 nm thick), electron-beam-evaporated Co films. The spin- and spatially-resolved surface magnetic structure (SMS) of the nano-scale Co elements is imaged *in situ* by using scanning ion microscopy with polarization analysis (SIMPA). SIMPA spin maps directly reveal the detailed spin structure of magnetic vortex and antivortex states, which can be utilized for ultra-high density, non-volatile magnetic memory devices. It is found that the SMS of the nano-magnetic structures depends strongly on the size of the patterned Co elements. In addition, FIB etching is utilized *in situ* to create well-defined defects (antidots) in the patterned Co elements, which strongly modify the previously existing SMSs leading to novel nano-magnetic states. The results show that ion–surface interaction, as provided by SIMPA spin mapping and *in situ* FIB processing, can be profitably exploited for studying SMSs of patterned magnetic systems to be used for nano-scale magnetic memory and magnetic logic devices.
© 2006 Elsevier B.V. All rights reserved.

PACS: 75.60.Ch; 75.75.+a; 75.70.Rf; 81.16.Nd

Micromagnetic states in patterned magnetic films are attracting much attention, not only because of the fundamental interest in new physical phenomena, but also because they are of their pivotal importance for the development of highly sophisticated magnetic devices, such as magnetic random accessory memory (MRAM), magnetic reading and writing heads, magnetic sensor arrays and magnetically controlled logic devices. It is found that switching fields and switching behavior in patterned magnetic elements depend strongly on these micromagnetic states. Much theoretical and experimental effort is being spent to explore micromagnetic states in patterned magnetic films, which are often based on soft magnetic materials, such as polycrystalline Co and NiFe [1–6]. The existence of S, C, flower, edge-pinning, vortex, antivortex and other micromagnetic states has been reported [1–11]. Among these micromagnetic states, magnetic vortex and antivortex states in circular elements have become more and more important, not only because of they possess reduced magnetic stray fields, which allow for higher storage densities, but also because they are predicted to possess a three-dimensional, curling magnetic structure where the magnetization near the vortex core turns out of the surface plane due to magnetic effects caused by exchange interactions [6,7].

Using magnetic force microscopy (MFM), Shinjo et al. [6] studied the magnetic structure of small circular permalloy dots and found that in the center of the dots, nm-sized turned-up or turned-down magnetization components, which reveal the existence of magnetic vortex cores. Measuring surface magneto-optical Kerr effect (SMOKE) hysteresis loops at surfaces of patterned permalloy and supermalloy elements and using micromagnetic simulations, Cowburn et al. [10] and Shi et al. [8,9] were able to

* Corresponding author. Tel.: +1 713 348 5417; fax: +1 713 348 4150.
  E-mail address: rau@rice.edu (C. Rau).

identify indirectly the existence of magnetic vortices in these patterned elements. Using Lorentz microscopy (LM), Raabe et al. [12] and Schneider et al. [13] explored the nucleation and propagation of magnetic vortices in circular Co and permalloy disks. Using scanning electron microscopy with polarization analysis (SEMPA), which utilizes electron–surface interaction to obtain information about surface magnetic structures (SMSs), Vaz et al. found that circular, epitaxial fcc Co(001) disks exhibit a magnetic vortex structure with a nearly closed-flux, four quadrant magnetic domain, typical of a system with cubic anisotropy with uniform surface magnetism inside each quadrant domain [14].

Using scanning ion microscopy with polarization analysis (SIMPA), which utilizes ion–surface interaction to investigate SMSs, we report on the experimental observation and *in situ* modification of the detailed spin- and spatially-resolved SMS of magnetic vortex and antivortex states in circular (diameter $d = 5$–38 μm), thin (thickness $D = 30$ nm), polycrystalline Co disks with negligible magnetocrystalline anisotropy, where predominantly the competition between exchange and demagnetizing fields should be responsible for the basic structure of the micromagnetic states. From spin- and spatially-resolved SIMPA spin maps, it is found that, depending on the diameter d of the elements, the detailed SMS consists completely of single or multi-vortex states. The magnetic vortex and antivortex states possess a circular or hyperbolic SM profile, respectively, with a central vortex or antivortex core (circular or cross Bloch lines) with far extended tails of the out-of-plane component of the surface magnetization (SM).

Well-defined defects (antidots) in the circular magnetic elements are introduced by *in situ* focused ion beam (FIB) etching in order to remove the high-energy core of the vortex or antivortex states and to create wide or narrow Co ring elements with reduced out-of-plane components of the SM. This results in the collapse of the vortex or antivortex states and creates new, highly stable SMSs such as onion-shaped states with predominantly in-plane components of the SM.

Polycrystalline Co films (30 nm thick) were produced on Si(100) substrates by using electron beam evaporation at a rate of 0.03 nm/s [15]. The Co/Si(100) samples are inserted in a UHV chamber, and longitudinal SMOKE measurements are recorded. From all samples studied so far, perfectly square magnetic hysteresis loops with a low coercivity field $H_c = 14.8$ Oe $= (1.178$ A/m) are found. No changes of size and shape of the square loops are observed upon rotation of the samples around the surface normal, which indicates the presence of zero or randomly oriented magnetocrystalline anisotropy due to the very good polycrystalline nature of the Co films implying that effects of magnetocrystalline anisotropy are averaged out due to the small grain size. Therefore, these films should possess a very small reduced anisotropy constant Q given by $Q = K_r/K_d$, where K_r is an appropriate residual anisotropy coefficient and K_d is the stray field energy coefficient.

For $K_r = H_c M_s/2\mu_0$, $K_d = M_s^2/2\mu_0$ and $M_s = 1.4 \times 10^6$ A/m, we obtain $Q = H_c/M_s = 8.4 \times 10^{-4}$.

Subsequently, the samples are transferred *in situ* from the SMOKE chamber to the SIMPA microscope [11,16], which is located in an UHV chamber operating in the low 10^{-10} Torr region. SIMPA utilizes ion–surface interaction to retrieve information about SMSs. In SIMPA, a micro-focused (spot size: 35 nm) Ga^+ ion beam is scanned across a magnetic/nonmagnetic surface causing the emission of spinpolarized/non-spinpolarized electrons [11,16]. The electrons emitted from the sample surface are collected by using an extracting lens system and a Mott polarimeter operating at 20 keV. The electron spin polarization (ESP) is determined by measuring the asymmetry in electron count rates in channeltron detectors during 120° backscattering of spin-up and spin-down polarized electrons from a high-Z material. The SIMPA technique offers some unique advantages compared to many other magnetic imaging techniques, because of its capability to produce vectorial maps of the SMS by directly measuring the spatially-resolved vector orientation and magnitude of the ESP, which is directly proportional to the magnitude and orientation of the SM of the local surface area probed by the focused ion beam [16]. The inelastic mean free path of the emitted electrons amounts to only a few monolayers (ML) [17], which explains the high surface sensitivity of SIMPA. For a probing depth of less than 1 nm and a beam spot size of 35 nm, the amount of magnetic material probed by SIMPA amounts to about 10^4 magnetic atoms, which shows the extreme sensitivity of SIMPA as a surface magnetometer. At present, we are analyzing predominantly the two in-plane components of the SM by detecting the two in-plane components of the ESP of the emitted electrons. We note that the magnitude and orientation of the out-of-plane component P_z of **P** can be independently measured and confirmed. For this purpose, the sample is rotated 45° around the y-axis, and P_z is obtained from $P_x^{45} = (P_x^0 - P_z^0) \times 0.707$, with P_x^0 being the x component of **P** before rotating. A topographic image of the scanned surface is simultaneously obtained by using the sum of the electron count rates. For fast adjustment of imaging parameters, and precise location of areas to be imaged, a conventional electron detector is used to collect secondary electrons and allows for display of topographic images on a TV monitor at TV rates.

Comparing SIMPA with other magnetic techniques, we note that SIMPA is directly measuring the spin distribution of the SMS of magnetic elements, whereas MFM utilizes magnetic stray field mapping by measuring the contrast between different magnetostatic forces, which is sensitive to the magnitude of the applied magnetic field and which could modify the intrinsic SMSs [18]. LM exploits the magnetic contrast obtained from the deflection of electrons due to the Lorentz force during transmission through the magnetic induction in thin magnetic samples. Raabe et al. [12] and Schneider et al. [13] explore magnetization patterns obtained from Co disks and find, from Fresnel images, that

the dark or the bright, nm-sized spot in the center of the disk reflects the vortex structure of the SM oriented clockwise or anticlockwise, respectively.

Circular-shaped magnetic disks of sizes between 5 μm and 38 μm are fabricated by FIB etching. The magnetic structures are then studied *in situ* by using SIMPA [11,16,19,20]. For SIMPA imaging, typical ion currents are in the range of 0.08 nA, whereas for ion beam milling typical currents are in the nA range. For further details on FIB etching and SIMPA spin mapping, we refer to [11,19,20], where the SMS of magnetic C, S and cross-tie states is studied.

Fig. 1 shows a spin- and spatially-resolved SIMPA spin map obtained a the surface of a FIB-created, circular (diameter $d = 8$ μm), Co (30 nm thick)/Si(100) element.
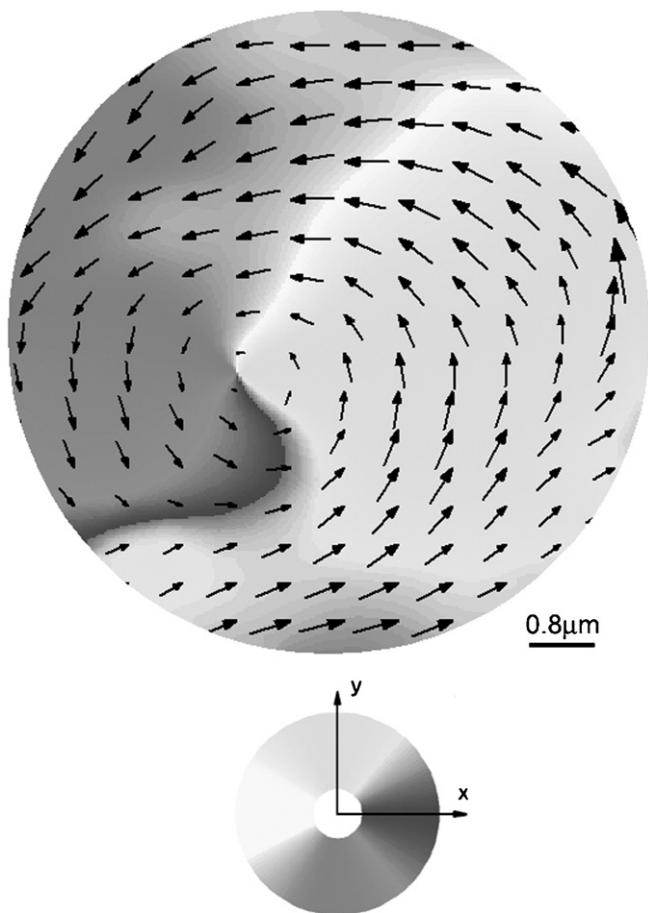

Fig. 1. A spin- and spatially-resolved SIMPA spin map obtained a the surface of a FIB-created, circular ($d = 8$ μm), Co ($D = 30$ nm)/Si(100) element. The grey shades in the image represent different orientations of the in-plane polarization P as given by the grey shade wheel (used for all figures) shown in the lower part, where also y and x axes are denoted with the z axis being normal to the x–y plane. The local orientation and magnitude of the P vectors is given by black arrows (used for all figures), the magnitude of P being proportional to the length of the arrows. In order to obtain a clear plot of the P vectors and to account for statistical fluctuations in electron count rates, for all spin maps, P is averaged over four nearest neighboring points and then only every forth P vector is plotted, thereby reducing the density of P vectors by a factor of 16.

The grey shades in the image represent different orientations of the in-plane ESP P as given by the grey shade wheel, which is shown in the lower part of Fig. 1 and which is used for all figures. For all figures, the local orientation and magnitude of the in-plane P vectors is given by black arrows, the magnitude of P being proportional to the length of the arrows. From the distribution of the P vectors, it is clearly visible that the SMS is *non-uniform* and exhibits predominantly circular in-plane components. Due to the negligible magnetocrystalline anisotropy of the elements, no domain walls with uniform domains between them are found. The *curling* of the P vectors directly reveals the single vortex structure of the SMS. From Fig. 1, it is clearly visible, that the magnitude of the in-plane ESP decreases with decreasing distance to the center of the vortex, where it becomes zero, indicating, with the assumption that the magnitude of the total ESP is constant, the existence of an increasing out-of-plane component of the ESP, which, at the center of the vortex, points perpendicularly out of the surface plane. Note that the existence of nonzero out-of-plane components of the ESP is expected to result from the competition between exchange and magnetostatic energies in magnetic materials with negligible anisotropy energy. Further, the existence of such unexpectedly wide extended tails of the SM in magnetic materials is consistent with the findings of Riedel and Seeger [21], who verified in a micromagnetic treatment of Néel-type walls, the existence of unexpectedly far extended tails of the SM for soft magnetic materials. Hubert and Schäfer [1] give an estimate for the tail width W, which is determined by a balance between K_d and K_r. For $W = 0.56 \, DK_d/K_r = 0.56 \, D/Q$ with D being the thickness of the film, we obtain $W = 20$ μm.

In order to study multi-vortex and antivortex states, the diameter d of the Co elements is varied between 5 and 38 μm. For d values above 13–15 μm, multi-vortex states including antivortex states become dominant. Fig. 2(a) gives a SIMPA spin map of an FIB-created Co element for $d = 25$ μm. From Fig. 2(a), antivortex and vortex states with hyperbolic and circular magnetization profiles can be directly identified. Fig. 3(b) shows an enlarged spin map of an antivortex state located in the lower left part of Fig. 2(a) (see white-dashed rectangle in Fig. 2(a)). From this, the hyperbolical profile of the SMS is clearly visible with the magnitude of in-plane P vector component decreasing with decreasing distance to the center of antivortex, indicating the presence of increasing out-of-plane components of P towards the center of the antivortex.

Fig. 3(a) gives a SIMPA spin map of an FIB-created Co element for $d = 10$ μm. A single vortex structure, similar to that shown in Fig. 1, is clearly visible. In next SIMPA experiments, we insert antidots (holes) into the Co element by using FIB etching. Fig. 3(b) gives a SIMPA spin map obtained after FIB etching of a hole (antidot) with $d_i = 3$ μm close to the center of the 10 μm-diameter Co ring element shown in Fig. 3(a). After remagnetization, the SMS is measured in the demagnetized state. From the spin
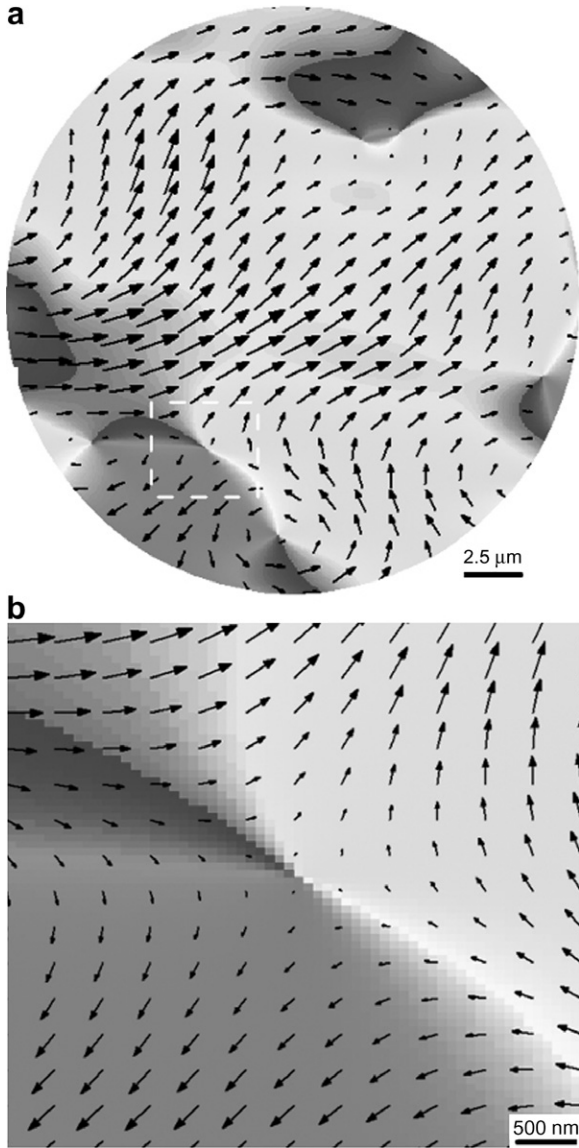
Fig. 2. (a) SIMPA spin map obtained at the surface of a FIB-created, circular ($d = 25\ \mu m$) Co element. (b) Enlarged SIMPA spin map of the magnetic antivortex located in the lower left part of (a) (see white-dashed square).

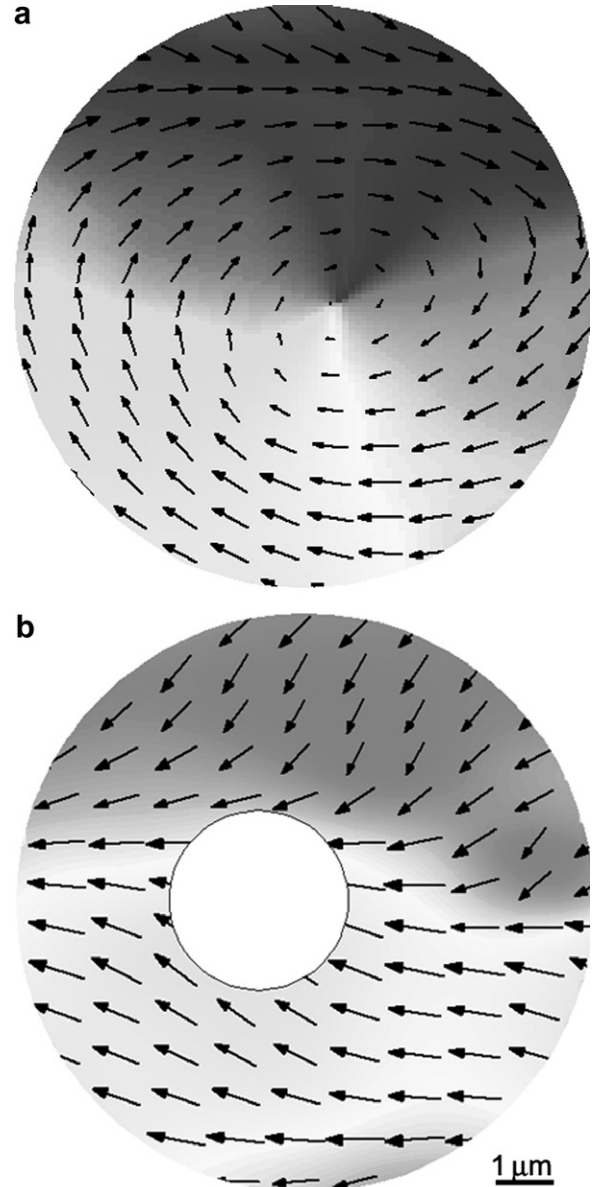Fig. 3. (a) SIMPA spin map of a circular Co circular disk element with $d = 10\ \mu m$. (b) SIMPA spin map of a circular Co ring element for $d = 10\ \mu m$ and $d_i = 3\ \mu m$.

map shown in Fig. 3(b), it is directly visible that the previous vortex structure, shown in Fig. 3(a), has collapsed into a SMS which is predominantly oriented in the surface plane and exhibits a so-called onion state (opposite circulation in each half of the ring). It is found that for small, FIB-etched holes (wide rings, $d_i/d < 0.15$), flux-closure, ring-shaped SMS structures are created, whereas for large, FIB-etched holes (narrow rings, $d_i/d > 0.3$), onion states are created. These findings directly show that FIB etching can be used to modify micromagnetic states in patterned magnetic systems.

It is shown that SIMPA provides and excellent means to study the detailed spin- and spatially-resolved SMS of *non-uniform* (curling) nano-magnetic states, such as magnetic vortices and antivortices, in patterned magnetic films. For circular-shaped, polycrystalline, patterned Co elements with negligible magnetocrystalline anisotropy, nano-magnetic states consist, depending on the diameter of the elements, of magnetic vortex, antivortex and multi-vortex states. The magnetic vortex/antivortex states possess circular/hyperbolic nano-magnetic profiles, respectively, with a central vortex/antivortex core with near completely perpendicular SMS and unexpectedly wide extended tails with nonzero out-of-plane components of the SM due to the small reduced anisotropy constant Q. The SMS of the circular Co elements is modified *in situ* by focused ion beam (FIB) etching, resulting in vortex-like or in onion-shaped states depending on the diameter of the hole (antidot). The results show that SIMPA spin mapping in combination with *in situ* FIB etching can develop into an important

and efficient tool to find desired, optimized micromagnetic states for patterned magnetic systems to be used for nano-scale magnetic memory and magnetic logic devices.

References

[1] A. Hubert, R. Schäfer, Magnetic Domains, Springer-Verlag, Berlin, Germany, 1998.

[2] Y. Zheng, J.-G. Zhu, J. Appl. Phys. 81 (1997) 5471.

[3] W. Rave, A. Hubert, IEEE Trans. Magn. 36 (2000) 3886.

[4] J. Shi, S. Tehrani, Appl. Phys. Lett. 77 (2000) 1692.

[5] M.E. Schabes, H.N. Bertram, J. Appl. Phys. 64 (1988) 1347.

[6] T. Shinjo, T. Okuno, R. Hassdorf, K. Shigeto, T. Ono, Science 289 (2000) 930.

[7] J. Miltat, A. Thiaville, Science 298 (2002) 555.

[8] J. Shi, S. Tehrani, M.R. Scheinfein, Appl. Phys. Lett. 76 (2000) 2588.

[9] J. Shi, J. Li, S. Tehrani, J. Appl. Phys. 91 (2002) 7458.

[10] R.P. Cowburn, D.K. Koltsov, A.O. Adeyeye, M.E. Welland, D.M. Tricker, Phys. Rev. Lett. 83 (1999) 1042.

[11] J. Li, C. Rau, J. Appl. Phys. 95 (2004) 6527.

[12] J. Raabe, R. Pulwey, R. Sattler, T. Schweinböck, J. Zweck, D. Weiss, J. Appl. Phys. 88 (2000) 4437.

[13] M. Schneider, H. Hoffmann, J. Zweck, Appl. Phys. Lett. 77 (2000) 2909.

[14] A.F. Vaz et al., Phys. Rev. B 67 (2003) 140405.

[15] W.C. Uhlig et al., J. Appl. Phys. 91 (2002) 6943.

[16] N.J. Zheng, C. Rau, Mater. Res. Soc. Symp. Proc. 313 (1993) 723.

[17] D.L. Abraham, H. Hopster, Phys. Rev. Lett. 58 (1987) 1352.

[18] J.M. García-Martín, A. Thiaville, J. Miltat, T. Okuno, L. Vila, I. Piraux, J. Phys. D: Appl. Phys. 37 (2004) 965.

[19] J. Li, C. Rau, J. Magn. Magn. Mater. 286 (2005) 473.

[20] J. Li, C. Rau, Nucl. Instr. and Meth. B 230 (2005) 518.

[21] H. Riedel, A. Seeger, Phys. Status Solidi B 46 (1971) 377.